

Energy analysis of 2D electro-thermo-hydrodynamic turbulent convection

Owen Hutchinson^a, Katerina Kostova^a, Jian Wu^b, Yifei Guan^{a,1}

^a*Department of Mechanical Engineering, Union College, Schenectady, 12308, NY, USA*

^b*School of Energy Science and Engineering, Harbin Institute of Technology, Harbin, 150001, China*

Abstract Turbulent convection is ubiquitous in fluid systems. In particular, multi-physical convection problems involve mass, heat, and particle transfer. When the particles are charged and driven by a high-voltage electric field, both buoyancy and electric forces contribute to driving and maintaining the convection. In this work, we perform numerical analysis using a high-fidelity Fourier-Chebyshev spectral solver. We further derive the dynamical systems governing the kinetic energy, the enstrophy, the potential energy, and the electric energy analytically. Using the simulated data, we apply a long short-term memory recurrent neural network to predict the chaotic time series of domain-average energy terms. Finally, we perform a data-driven modal decomposition to show the coherent structures that contain energy and enstrophy in 2D turbulent convection.

1. Introduction

Electro-hydrodynamics (EHD) is a multi-physical discipline that describes the three-way interactions between the charged particles, neutral molecules, and the electric field on a macroscopic scale, which involves fluid mechanics and electro-dynamics [1, 2, 3, 4, 5, 6, 7, 8, 9]. Additionally, electro-thermo-hydrodynamics (ETHD) involves one more complexity, the heat transfer or temperature field [10, 11, 12]. ETHD convection has been a research focus since its first introduction to model the geo-convection of the mantle [13, 14]. ETHD and EHD have since been analyzed in multiple backgrounds, e.g., solidliquid interface [15], Taylor

¹Corresponding author: guany@union.edu

cone [16], and enhanced heat transfer [17]. In recent years, many studies have focused on the linear stability analysis of the ETHD systems [18, 10] and transition routes to chaos [19, 20]. Despite the broad interest in the stability analysis of laminar or mildly chaotic ETHD convection, only a few studies have attempted to analyze the turbulent and highly chaotic (high Rayleigh number, Ra , and high electric Rayleigh number, T) regimes [21, 22]. In particular, the recent paper of our group presents the relationship between the potential energy and electric energy budgets and the kinetic energy dissipation [22].

The numerical study of ETHD convection flows is routinely performed with high-fidelity numerical simulations [23, 24, 25, 26, 27, 28, 29, 30, 3, 22], resulting in a large amount of high-resolution spatio-temporal data. In spite of the high-dimensional nature of turbulent (highly chaotic) ETHD convection, many phenomena in electro-thermo-convection and other similar systems can be characterized by a few dominant coherent structures [31, 32, 33, 34], or *modes* as in modal analysis. High-fidelity simulations (e.g., direct numerical simulations or DNS) often obscure this simplicity, making optimization and control tasks prohibitively expensive [35]. Therefore, there is a need for accurate and efficient reduced-order models that describe ETHD turbulence, similar to the Lorenz model for Rayleigh-Bénard convection (RBC) [36]. The Lorenz model was obtained by Galerkin projection of the governing equations onto a reduced set of three Fourier modes that was earlier proposed by Saltzman [37]. Instead of extracting these modes manually (analytically), modes can also be extracted automatically (from data), for example via proper orthogonal decomposition (POD) [38, 39, 40, 31, 34] or dynamic mode decomposition (DMD) [34, 41]. Modal analysis also facilitates other practice such as flow control [42, 43, 44, 45, 46, 47, 48] and fluid-structure interaction analysis [49, 33].

In order to predict the temporal evolution of chaotic dynamical systems, recent advances focus on data-driven prediction: e.g., artificial neural network [50], reservoir computing [51, 52, 53, 54], and recurrent neural network (RNN) [55, 56]. In particular, the Long Short-Term Memory (LSTM) network is an RNN architecture designed to model temporal dependencies in sequential data. Different from conventional RNNs, which often suffer from vanishing or exploding gradients when learning long-range correlations, LSTMs introduce a gated structure, comprising input, output, and forget gates, that enables the selective retention and updating of information over extended time horizons. This capability makes LSTMs particularly effective for capturing nonlinear and dynamic patterns in time series, making them widely adopted in domains such as speech recognition, natural language processing, and scientific modeling of complex dynamical

systems [57, 58, 59].

In the current study, we follow up upon our recent work [22] to (1) derive the governing equations for kinetic energy, enstrophy, potential energy, and electric energy; (2) train LSTMs to predict the time series of domain-average kinetic energy, potential energy, and electric energy; (3) perform data-driven modal decomposition using the proper orthogonal decomposition (POD); and (4) compare the modal analysis and identify the coherent structures related to energy concentration.

The remainder of the paper is as follows. Section 2 presents the dimensionless governing equations of the original 2D ETHD system, and the derivation of the dynamical systems of the energy terms. It further describes the LSTM, 2D wavelet analysis, and POD analysis used in this work. Section 3 presents the numerical results. Conclusion and future work discussion are presented in Section 4.

2. Methodology

2.1. Governing equations of the ETHD system

The governing equations for ETHD convection system include the conservation of mass and momentum (Navier-Stokes equations with the electric and buoyancy forcing terms), the conservation of electrical current equation (transport of charge density), the Poisson equation for electric potential with the space-charge effect, and the conservation of potential energy equation (heat transport). The effects of viscous dissipation and the Joule heating on the thermal energy are neglected for simplicity. Following the Boussinesq approximation, the dimensionless governing equations can be written as: [e.g., 21, 19, 60, 22]

$$\nabla \cdot \mathbf{u} = 0, \quad (1)$$

$$\frac{\partial \mathbf{u}}{\partial t} + (\mathbf{u} \cdot \nabla) \mathbf{u} = -\nabla P + \nu \nabla^2 \mathbf{u} + F_E q \mathbf{E} + F_\theta \theta \mathbf{e}_y, \quad (2)$$

$$\frac{\partial q}{\partial t} + \nabla \cdot [q(\mathbf{u} + \mathbf{E})] = \nu_E \nabla^2 q, \quad (3)$$

$$\nabla^2 \phi = -Cq/4, \quad (4)$$

$$\mathbf{E} = -\nabla \phi, \quad (5)$$

$$\frac{\partial \theta}{\partial t} + \mathbf{u} \cdot \nabla \theta - u_y = \nu_\theta \nabla^2 \theta. \quad (6)$$

Here, $\mathbf{e}_y = (0, 1)$ is the unit vector pointing towards the y direction (opposite of gravity); $\mathbf{u} = (u_x, u_y)$ is the 2D velocity vector; p is the pressure scalar; $\mathbf{E} = (E_x, E_y)$ is the 2D electric field vector; θ is the temperature anomaly defined as the difference between the temperature and conductive temperature profile ($T_{\text{conduction}} = -y$); q is the net charge density; and ϕ is the electric potential. Note that all parameters are dimensionless [22].

The system is controlled by the initial and boundary conditions, together with the six dimensionless parameters: ν is the molecular viscosity; F_E is the electric forcing magnitude; F_θ is the buoyancy forcing magnitude; ν_E is the charged particle viscosity; C is the charge injection strength; and ν_θ is the thermal diffusivity.

2.2. Boundary conditions

The non-slip boundary condition ($\mathbf{u}_{y=\pm h} = 0$) are applied to the fluid flow at the upper ($y = h$) and lower ($y = -h$) planes. And the periodic boundary condition is applied to the lateral (x) direction. The boundary conditions of the other variables are listed as follows.

$$\phi_{y=-h} = 1, \quad \phi_{y=h} = 0, \quad (7)$$

$$q_{y=-h} = 1, \quad (\partial q / \partial y)_{y=h} = 0, \quad (8)$$

$$\theta_{y=\pm h} = 0. \quad (9)$$

In this work, we investigate 8 cases with the dimensionless parameters shown in Table 1.

In addition to these four parameters, the other two dimensionless governing parameters remain constants: $F_E = 250$ and $\nu_E = 2.00 \times 10^{-4}$. For Cases 1 and 5 where $C = 0$, the ETHD system reduces to the classical Rayleigh-Bénard Convection (RBC). The dimensionless parameters chosen here cover a broad range: $Pr \in [7, 100]$, $Ra \in [5 \times 10^7, 10^9]$, and $T \in [10^3, 4 \times 10^3]$, where Pr is the Prandtl number, Ra is the Rayleigh number, and T is the Taylor number or electric Rayleigh number [22].

Table 1: Dimensionless parameters governing the dynamics of the turbulent ETHD convection

Case	ν	F_θ	ν_θ	C	$\langle E_u \rangle_{V,t}$	$\langle \Omega \rangle_{V,t}$
1	0.050	1.12×10^3	7.14×10^{-3}	0	50.68	1792.90
2	0.050	1.12×10^3	7.14×10^{-3}	10	52.78	1891.20
3	0.033	4.96×10^2	4.76×10^{-3}	10	27.88	978.97
4	0.025	2.79×10^2	3.57×10^{-3}	10	21.85	722.85
5	0.10	6.25×10^3	1.00×10^{-3}	0	49.98	1558.30
6	0.10	6.25×10^3	1.00×10^{-3}	10	51.74	1598.10
7	0.050	1.56×10^3	5.00×10^{-4}	10	16.90	489.90
8	0.033	6.94×10^2	3.33×10^{-4}	10	12.34	340.15

2.3. Kinetic, potential, and electric energy and enstrophy equations

The kinetic energy, $E_u = \frac{1}{2}\mathbf{u}^2 = \frac{1}{2}(u_x^2 + u_y^2)$, can be obtained by multiplying the momentum equation by the velocity vector \mathbf{u} and domain averaging $\langle \cdot \rangle_V$:

$$\frac{\partial \langle E_u \rangle_V}{\partial t} = -\langle \epsilon_K \rangle_V + F_E \langle q\mathbf{u} \cdot \mathbf{E} \rangle_V + F_\theta \langle \theta u_y \rangle_V. \quad (10)$$

The enstrophy, $\Omega = \frac{1}{2}\omega^2$, where $\omega = \nabla \times \mathbf{u}$, can be obtained in a similar way:

$$\frac{\partial \langle \Omega \rangle_V}{\partial t} = -\langle \epsilon_\omega \rangle_V + F_E \langle \omega \nabla \times (q\mathbf{E}) \rangle_V + F_\theta \langle \omega \frac{\partial \theta}{\partial x} \rangle_V. \quad (11)$$

Here, $\langle \epsilon_K \rangle_V = \nu \langle \omega^2 \rangle_V$, and $\langle \epsilon_\omega \rangle_V = \nu \langle |\nabla \omega|^2 \rangle_V$ are energy and enstrophy dissipation terms.

The potential energy, $E_p = -F_\theta y(\theta - y)$, can be obtained by multiplying the equation for θ by y , followed by a domain averaging:

$$\frac{\partial \langle E_p \rangle_V}{\partial t} = F_\theta \nu_\theta (N_u - 1) - F_\theta \langle \theta u_y \rangle_V \quad (12)$$

Here, N_u is the Nusselt number that varies in time. The potential energy equation is consistent with the previous studies on Rayleigh-Bénard Convection [61, 62].

Similarly, the electric energy, $E_e = F_E q \phi$, can be obtained by multiplying the equation for q by ϕ , followed by a domain averaging:

$$\frac{\partial \langle E_e \rangle_V}{\partial t} = F_E \langle p_E \rangle_V - F_E \langle q \mathbf{u} \cdot \mathbf{E} \rangle_V \quad (13)$$

$$- F_E q \langle \nabla \phi \cdot \nabla \phi - \frac{\partial \phi}{\partial t} \rangle_V \quad (14)$$

$$- F_E \nu_E \langle \nabla \phi \cdot \nabla q \rangle_V. \quad (15)$$

Here, $\langle p_e \rangle_V = \Delta \phi I_0 N_e / H$ is the total electric energy injection into the ETHD system across the boundary, where $\Delta \phi$ is the electric potential difference between the lower and upper planes, and H is the height. $I_e = \langle \mathbf{i} \rangle_{A, y=-1}$ and $N_e = I_e / I_0$ is the electric Nusselt number. I_0 equals I_e at the hydrostatic state [63, 22].

The relation among the kinetic, potential, and electric energy can be summarized as follows.

$$\frac{\partial \langle E_u \rangle_V}{\partial t} = -D_u + \Phi_E + \Phi_\theta \quad (16)$$

$$\frac{\partial \langle E_p \rangle_V}{\partial t} = N_\theta - \Phi_\theta \quad (17)$$

$$\frac{\partial \langle E_e \rangle_V}{\partial t} = N_E - \Phi_E - D_{elec} \quad (18)$$

Here, $D_u = \langle \epsilon_K \rangle_V$ is the viscous dissipation; $\Phi_E = F_E \langle q \mathbf{u} \cdot \mathbf{E} \rangle_V$ is the electric energy transferred into kinetic energy; $\Phi_\theta = F_\theta \langle \theta u_y \rangle_V$ is the potential energy transferred into kinetic energy; $N_\theta = F_\theta \nu_\theta (N_u - 1)$ is the net potential energy injection by heat flux across the boundary; $N_E = F_E \Delta \phi I_0 N_e / H$ is the net electric energy injection by current flux across the boundary; and $D_{elec} = F_E q \langle \nabla \phi \cdot \nabla \phi - \frac{\partial \phi}{\partial t} \rangle_V + F_E \nu_E \langle \nabla \phi \cdot \nabla q \rangle_V$ is the electric dissipation [21, 22]. The domain-averaged kinetic energy, $\langle E_u \rangle_V$, and enstrophy, $\langle \Omega \rangle_V$, are shown in Table 1.

2.4. Numerical analysis: numerical simulation, data-driven prediction, and coherent structure of energies and enstrophy with 2D wavelet decomposition and POD

Direct numerical simulation (DNS) solves Eqs. (1)- (6) using a Fourier-Chebyshev spectral solver at high spatial-temporal resolution, as described in our recent paper [22]. Specifically, the computational domain is $[x, y] \in [0 : 4, -1 : 1]$. The flow is periodic in the horizontal (x -) direction and wall-bounded (no-slip) in the

vertical (y -) direction. The spatial derivative in the periodic horizontal direction is solved by the Fourier pseudo-spectral method, and the spatial derivative in the wall-normal direction is solved using the Chebyshev differential matrices [e.g., 64]. The temporal advancement is solved using the 2^{nd} -order AdamsBashforth method for the convection/advection terms, and the semi-implicit CrankNicolson method for the diffusion terms [65, 60]. The DNS timestep size is taken to be $\Delta t = 10^{-5}$ for all simulations. The vorticity (ω) - stream function (ψ) formulation is used to represent the flow field, and the multiphysical convection is driven by heat transport, charge transport, and electric potential equations.

2.4.1. Predicting the time series of domain-averaged energy equations using LSTM

The dynamical system described by Eqs. (16)-(18) represents the temporal evolutions of $\langle E_u \rangle_V$, $\langle E_p \rangle_V$, and $\langle E_e \rangle_V$. However, the algorithmic form of this system cannot be easily derived due to the complex relationships between the right-hand-side terms (e.g., D_u , N_θ , etc) and the three left-hand-side variables (i.e., $\langle E_u \rangle_V$, $\langle E_p \rangle_V$, and $\langle E_e \rangle_V$). Here, we aim to test the prediction performance of the LSTM recurrent neural network in predicting the temporal evolutions of $\langle E_u \rangle_V$, $\langle E_p \rangle_V$, and $\langle E_e \rangle_V$ from previous timesteps of $\langle E_u \rangle_V$, $\langle E_p \rangle_V$, and $\langle E_e \rangle_V$ only. In this work, we apply a single-layer LSTM with a varying number of neurons (n_{neuron}) in the hidden layer (LSTM layer). We investigate the prediction accuracy over a range of look-back timesteps, Δ_{back} (the number of timesteps used for prediction), prediction horizon, $\Delta_{forward}$ (the number of timesteps forward predicted by the LSTM), and other hyperparameters such as batch size and n_{neuron} . Here, the data separating timestep $\Delta = 0.01 = 10^3 \Delta t$.

2.4.2. 2D wavelet decomposition

To prepare the data for data-driven model decomposition (i.e., POD), we first project the energy data (i.e., E_u , E_p , E_e) and the enstrophy data (Ω) from the Chebyshev grid to a uniform grid in the wall-normal (y) direction [66]. Next, we perform 2D wavelet decomposition and obtain the filtered snapshots (approximation) of E_u , E_p , E_e , and Ω at the second level such that the spatial resolution is reduced by 4 in each of the x and y directions [67], which can be obtained using the *wavedec2* function in MATLAB [68]. The conceptual algorithm is described as follows, with $E_u(x, y)$ as an example.

$$E_u(x, y) = A_1 + H_1 + V_1 + D_1, \quad (19)$$

where A_1 is the *approximation*, H_1 is the *horizontal detail*, V_1 is the *vertical detail*, and D_1 is the *diagonal detail* matrices all at the first level. The decomposition is performed using a low-pass filter and a high-pass filter, and in this work, we use the basic Haar wavelet (Haar filters). To further perform multiscale analysis, the *approximation* A_1 can be further decomposed in a similar way:

$$A_1 = A_2 + H_2 + V_2 + D_2, \quad (20)$$

where A_2 , H_2 , V_2 , and D_2 are corresponding matrices at the second level [67].

2.4.3. Proper orthogonal decomposition (POD)

To perform POD of the energy and enstrophy data, we first concatenate all snapshots of each of E_u , E_p , E_e , and Ω into a matrix \mathbf{X} , e.g., for E_u :

$$\mathbf{X} = [E_u(0), E_u(\Delta t), E_u(2\Delta t), \dots, E_u(n_t\Delta t)], \quad (21)$$

where $E_u(j\Delta t)$, $j = 0, 1, \dots, n_t$ is a column vector with a dimension reshaped from $[n_x, n_y]$ to $[n_x \times n_y, 1]$, n_t is the number of snapshots, n_x and n_y are the dimensions of the grid in the original two directions x and y , and Δt is the time difference in each two consecutive snapshots. POD of E_u is obtained by performing a reduced singular value decomposition (reduced SVD) of \mathbf{X} : $[U, S, V^T] = \text{svd}(\mathbf{X}, \text{"econ"})$ [69, 41, 34]. Here, matrix U contains POD modes that contain spatial information (each column of U is a reshaped POD mode), diagonal matrix S contains the magnitude of each mode, and matrix V contains their corresponding temporal evolution dynamics (each column of V is a temporal evolution dynamic).

3. Results

Table 1 shows the domain and time averaged kinetic energy and enstrophy for the 8 cases. It can be observed that for constant parameters, the electric field has a positive impact on both kinetic energy and enstrophy, by comparing Cases 1 and 2 or Cases 5 and 6. However, when F_θ decreases, both the kinetic energy and the enstrophy decrease.

Next, we investigate the spatial and temporal distribution of the energy terms E_u , E_p , and E_e . Figure 1 shows the snapshots of E_u , E_p , and E_e and their corresponding 2D wavelet approximation at the second level (A_2 as in Eq. (20)). It

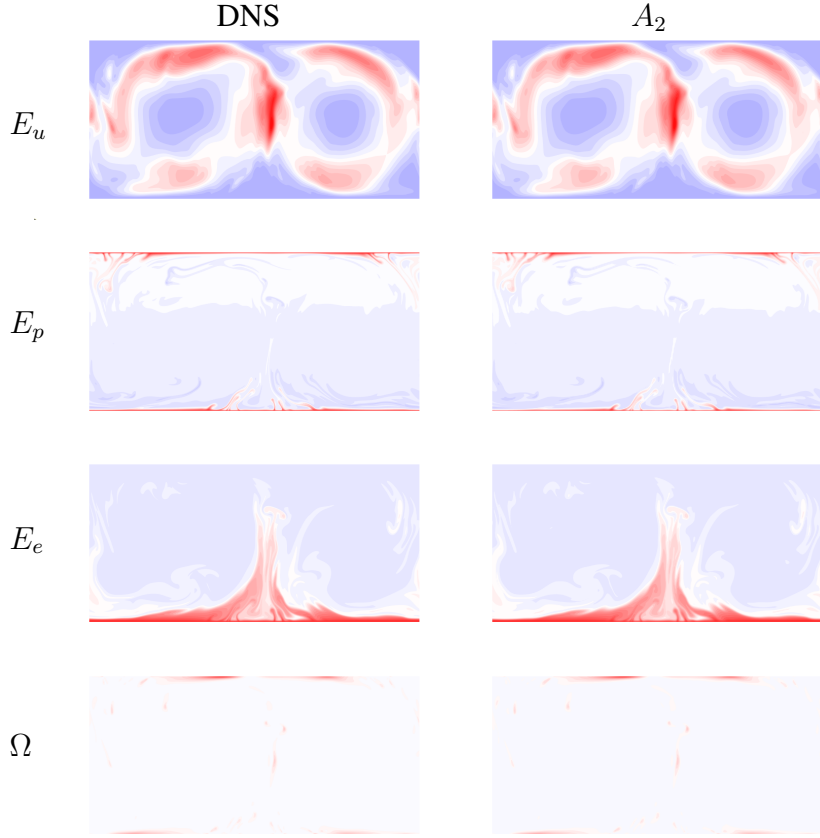


Figure 1: The DNS snapshots and their 2D wavelet approximations at the second level (A_2) of E_u , E_p , E_e , and Ω for Case 8.

can be observed that A_2 matches the DNS snapshots structurally, albeit using $16\times$ lower resolution. In fact, as shown in Fig. 2, the domain-average values $\langle E_u \rangle_V$, $\langle E_p \rangle_V$, and $\langle E_e \rangle_V$ obtained from the approximation A_2 also match the DNS well, meaning that the energies are primarily contained in the large scales. It further justifies our choice of using 2D wavelet decomposition to approximate the energy distribution in 2D ETHD systems.

As we have the temporal evolution of $\langle E_u \rangle_V$, $\langle E_p \rangle_V$, and $\langle E_e \rangle_V$ representing the dynamical system mathematically described in Eqs. (16), (17), and (18), we investigate the performance of a single-layer LSTM in prediction. Here, we use the time series shown in Fig. 2 normalized by their corresponding temporal average (i.e., $\langle E_u \rangle_V / \langle E_u \rangle_{V,t}$, $\langle E_p \rangle_V / \langle E_p \rangle_{V,t}$, and $\langle E_e \rangle_V / \langle E_e \rangle_{V,t}$) as training and validation data. Here, we use the time series in $t \in [0, 80]$ as training data set,

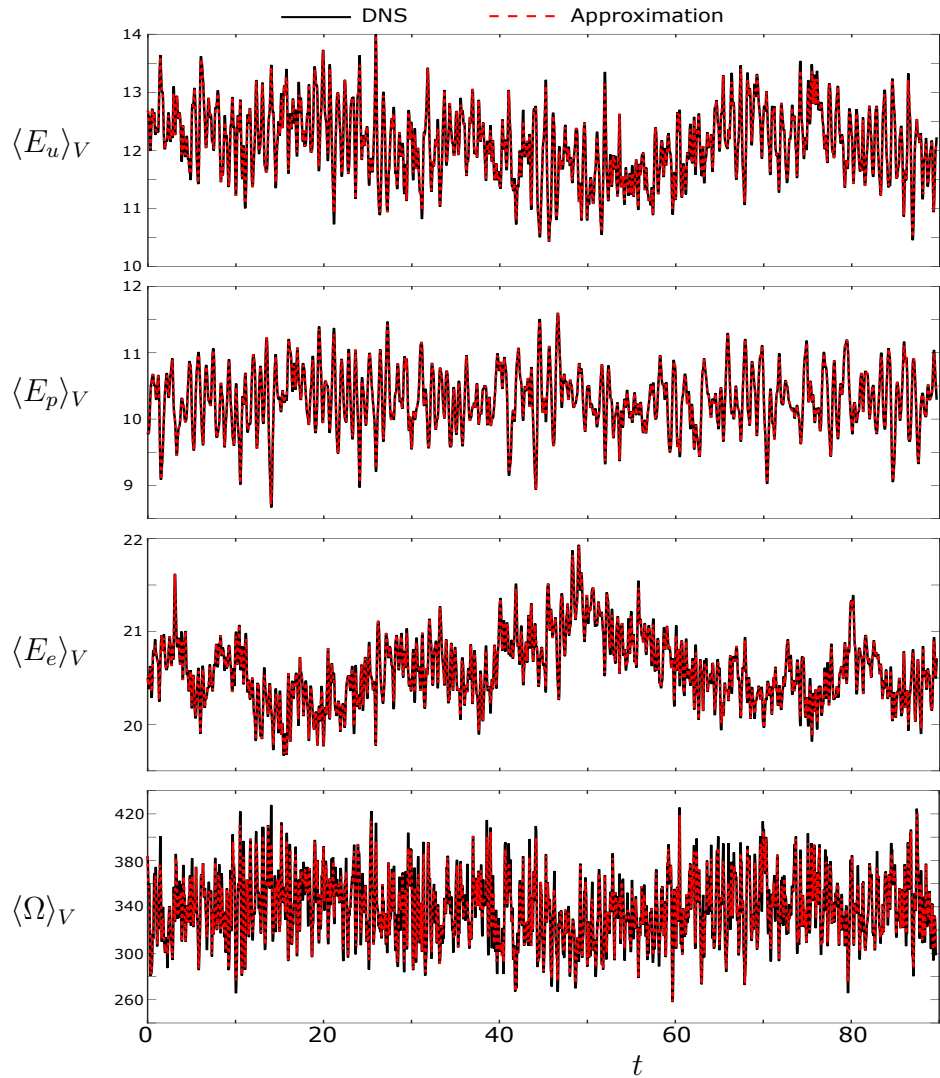


Figure 2: The domain-averaged DNS energy and enstrophy and their 2D wavelet approximations at the second level of E_u , E_p , E_e , and Ω for Case 8. The domain-averaged values vary in time, t .

$t \in (80, 85]$ as validation data set, and $t \in (85, 89.4]$ as testing data set. Figure 3 shows the training processes from a variety of single-layer LSTMs with different hyperparameters Δ_{forward} , Δ_{back} , n_{neuron} , and batch size. Figure 3 (a) shows the training loss and validation loss over epochs (training iterations). In most cases, the training is converged within 60 epochs. Figure 3 (b) shows the effects of the prediction horizon Δ_{forward} and the number of look-back timesteps Δ_{back} . It can be observed that a smaller Δ_{forward} leads to higher prediction accuracy (lower \mathcal{L}), which is intuitive because the closer the future is, the easier it is to predict. However, Δ_{back} does not follow “the more the better” rule. Here, we use $\Delta_{\text{back}} = m\Delta_{\text{forward}}$, and find that $m = 5$ actually performs better than $m = 3$ or $m = 10$ in terms of reducing the validation loss. Figure 3 (c) shows the effects of n_{neuron} , and we find that $n_{\text{neuron}} = 512$ works well in all cases. A small n_{neuron} may lead to underfitting and a large n_{neuron} may lead to overfitting, which both will deteriorate the validation loss. Figure 3 (d) shows the effects of batch size, and we find that batch size = 16 or 32 works well for all cases. In general, to balance the prediction horizon and accuracy, we use $\Delta_{\text{forward}} = 10$, $\Delta_{\text{back}} = 10\Delta_{\text{forward}}$, $n_{\text{neuron}} = 512$, and batch size = 32 for the next analysis, which is shown in Fig. 4.

The LSTM testing results are shown in Fig. 4. The testing data set has not been seen during the training process, as the LSTM is trained on the training data, and the stopping criteria and the optimization are based on the validation data. The testing data set is used for testing the prediction performance only. It can be seen from Fig. 4 that the prediction (forecast) matches the truth (true future) very well using the LSTM in the prediction horizon (10Δ), where $\Delta = 10^3\Delta t$ is the data separating timestep. It should be noted that the prediction horizon shown in Fig. 4 includes an extreme value (local minimum in $\langle E_u \rangle$ or maximum in $\langle E_p \rangle$ and $\langle E_e \rangle$), which shows the capability of the LSTM to predict not only monotonic behavior but also to correctly predict extreme values in a chaotic time series. Although the prediction horizon seems to be short compared with the full time series, it should be noted that the prediction horizon here is equivalent to $10^4\Delta t$, where Δt is the DNS timestep size.

The temporal evolution of domain-average values shows how energies vary over time. However, the spatial distribution information is lost when the domain average is applied. Next, we investigate the spatial distribution of the energy and enstrophy terms by showing the results of POD modal analysis of E_u , Ω , E_p , and E_E of Case 8, as shown in Fig. 5. It can be observed that for all the energy-related properties, the first POD mode captures the large-scale dynamics (coherent structures) of the corresponding energy. For kinetic energy E_u , the

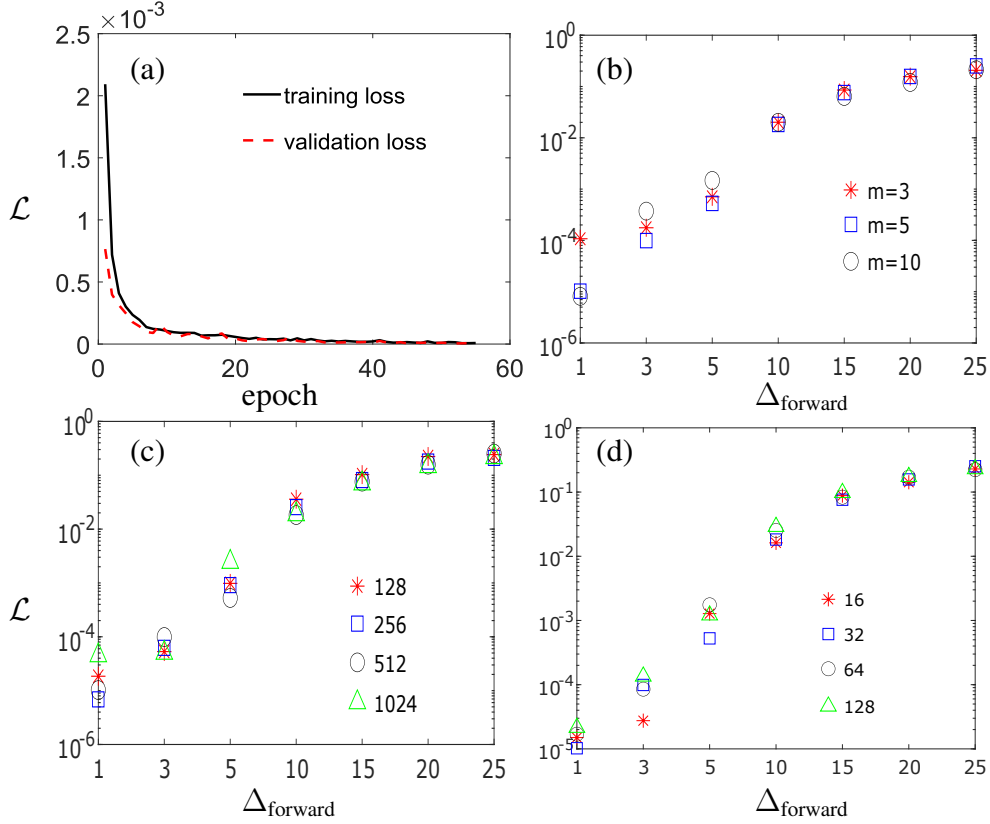


Figure 3: (a) The training and validation loss \mathcal{L} for Case 8 with $\Delta_{\text{forward}} = \Delta$, $\Delta_{\text{back}} = 10\Delta_{\text{forward}}$, $n_{\text{neuron}} = 256$, and batch size = 32; (b) the minimum validation loss ($\min(\mathcal{L})$) with respect to Δ_{forward} and $\Delta_{\text{back}} = m\Delta_{\text{forward}}$ with $n_{\text{neuron}} = 512$, and batch size = 16; (c) $\min(\mathcal{L})$ with respect to Δ_{forward} and $n_{\text{neuron}} = [128, 256, 512, 1024]$ with $\Delta_{\text{back}} = 5\Delta_{\text{forward}}$ and bath size = 16; and (d) $\min(\mathcal{L})$ with respect to Δ_{forward} and batch size = [16, 32, 64, 128] with $\Delta_{\text{back}} = 5\Delta_{\text{forward}}$ and $n_{\text{neuron}} = 512$.

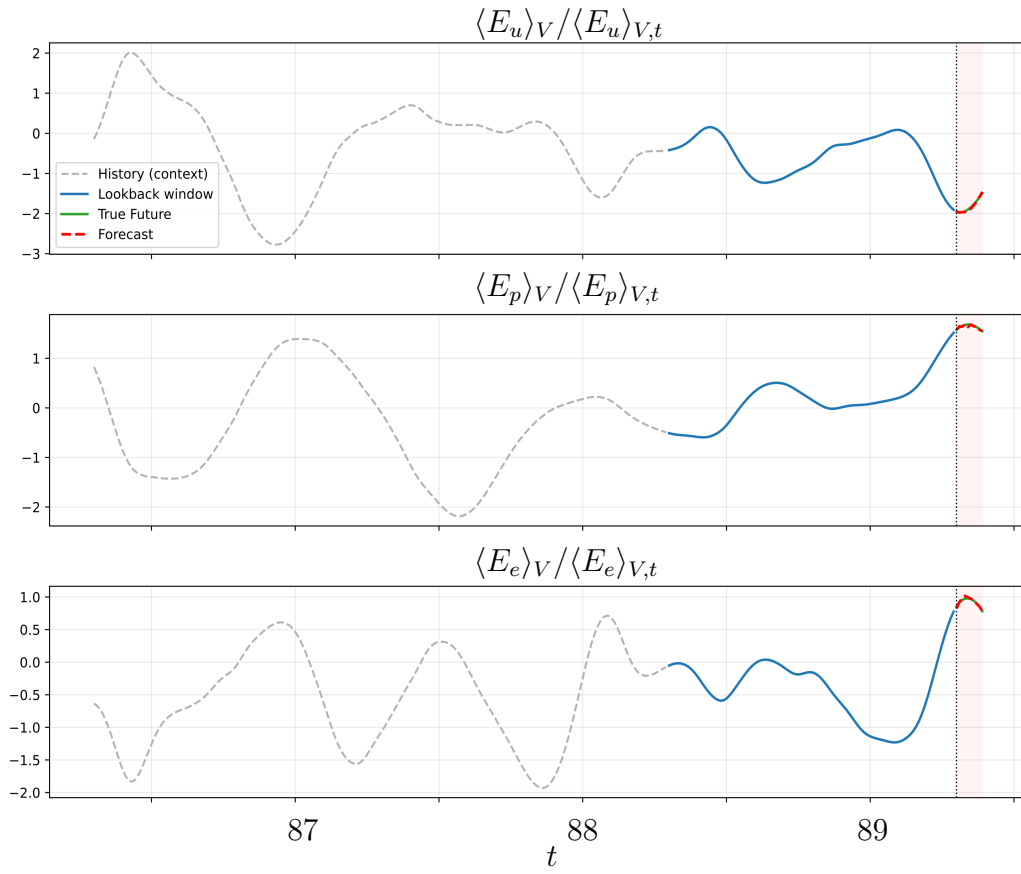


Figure 4: Prediction of the normalized time series $\langle E_u \rangle_V$, $\langle E_p \rangle_V$, and $\langle E_e \rangle_V$. The LSTM has $\Delta_{\text{forward}} = 10\Delta$, $\Delta_{\text{back}} = 10\Delta_{\text{forward}}$, $n_{\text{neuron}} = 512$, and batch size = 32.

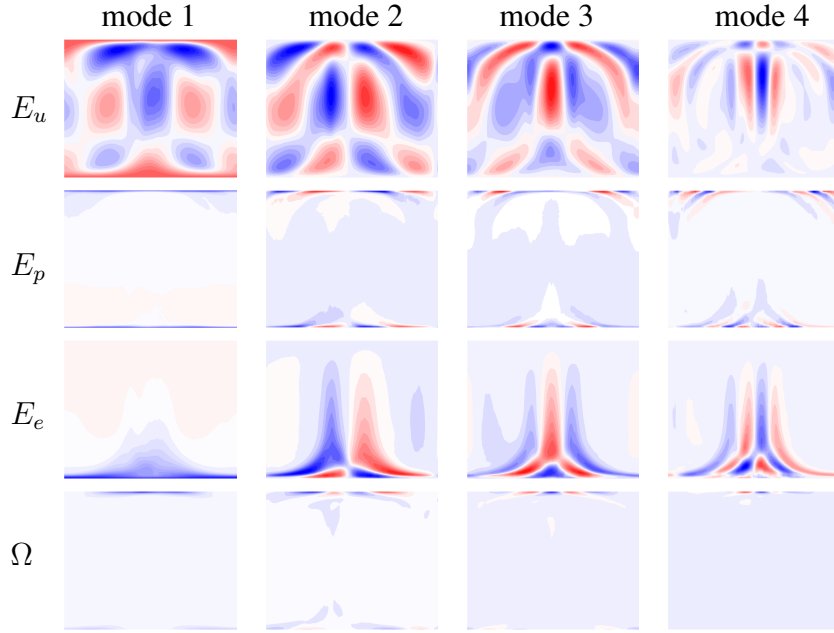


Figure 5: The first 4 POD modes of E_u , E_p , E_e , and Ω for Case 8.

first three modes contains energy in the large scales. For E_p , E_e , and Ω , small-scale structures (with smaller wave length in x) starts to emerge from mode 2. Also, the potential energy is more evenly distributed within the whole domain, while the electric energy is more concentrated in the plume. The findings here are consistent with our previous results on Φ_θ and Φ_E [22]. It should also be noted that Ω is heavily distributed within the boundary layer near the upper and lower walls. This is because in 2D flow field, enstrophy Ω is directly related to the viscous dissipation which is maximum near the wall due to the high velocity gradient [70, 71, 22].

In addition to the spatial distribution of energy and enstrophy, POD analysis also demonstrates the correlation between different modes obtained from different quantities. Figure 6 shows the correlation between the modal coefficients of E_p , E_e , and Ω with E_u . It can be observed that these modal coefficients are highly correlated (with correlation coefficients above 0.9), forming an almost linear relationship. This is particularly interesting, as it suggests that given a few leading modes, E_p , E_e , and Ω can be reconstructed by knowing or correctly predicting the coefficients of E_u modes only.

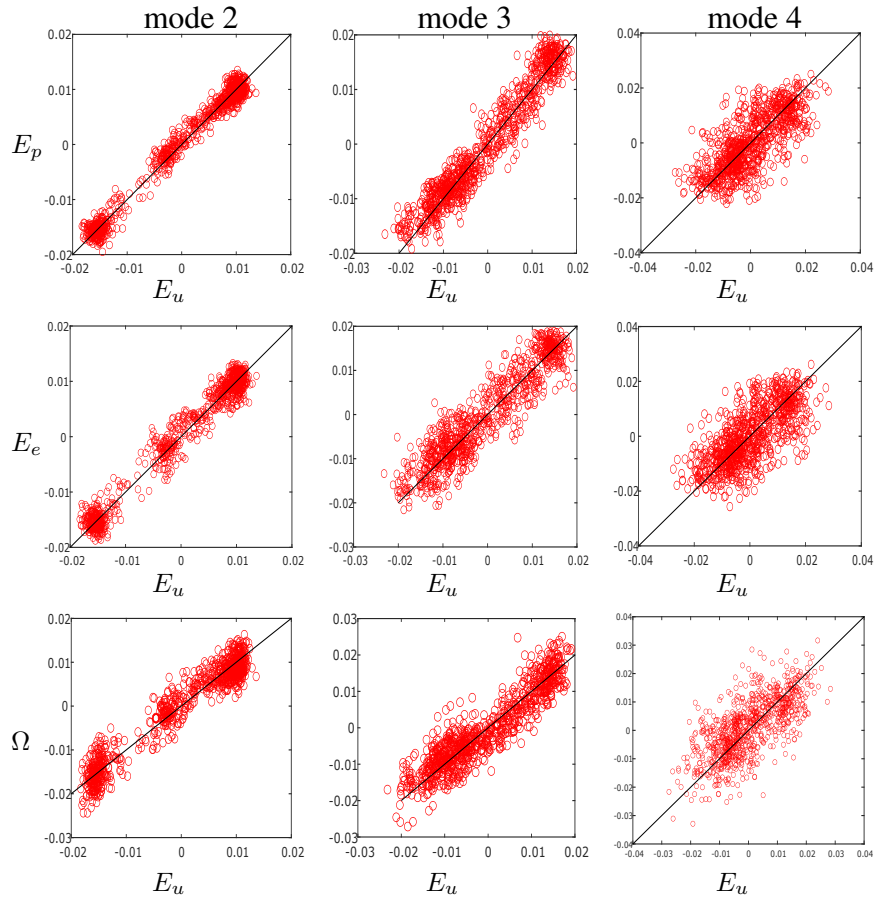


Figure 6: The correlation between the 2nd, 3rd, and 4th POD mode coefficients (columns of the matrix V) of E_p , E_e , and Ω with E_u for Case 8. The black lines represent the linear fit.

4. Conclusion

In this work, we analyze the energy terms in 2D ETHD turbulent convection systems. We first derive the governing equations (as in a dynamical system) of the kinetic energy, potential energy, and electric energy. We then remark the transitional terms (Φ_θ and Φ_E), which are the different contributions to kinetic energy due to potential energy and electric energy. This analysis completes the energy transfer picture described earlier in our previous work [22], and it is firstly reported in this work.

Next, we investigate a variety of single-layer LSTMs in predicting the time series of domain-average kinetic energy, potential energy, and electric energy. We show the capability of LSTM to predict up to $10^4 \Delta t$ accurately and predict the local extreme values accurately.

Furthermore, we perform POD analysis on the energy and enstrophy terms and show that the coherent structure that contains the energy can be well described by the first POD mode. We also investigate the correlation of modal coefficients between different energy/enstrophy terms and find that they form a linear relationship. However, due to the same feature, POD analysis cannot reveal the information contained in small structures which may be important for turbulent modeling using e.g., large eddy simulations.

In our future work, we aim to extend our modal analysis by using different data-driven modal analysis, such as dynamic mode decomposition (DMD), empirical mode decomposition (EMD), and variational mode decomposition (VMD), and compare their performance on analyzing the energy in a 2D ETHD turbulence system.

5. Acknowledgment

The authors appreciate the discussion with Dr. Mengqi Zhang, Dr. Qi Wang, and Dr. Yu Zhang on the chaotic ETHD systems.

References

- [1] N Felici and JC Lacroix. Electroconvection in insulating liquids with special reference to uni-and bi-polar injection: a review of the research work at the

- cnrs laboratory for electrostatics, grenoble 1969–1976. *Journal of Electrostatics*, 5:135–144, 1978.
- [2] Antonio Castellanos. *Electrohydrodynamics*, volume 380. Springer, 2014.
- [3] Lei Wang, Zhouchao Wei, Tianfu Li, Zhenhua Chai, and Baochang Shi. A lattice boltzmann modelling of electrohydrodynamic conduction phenomenon in dielectric liquids. *Applied Mathematical Modelling*, 95:361–378, 2021.
- [4] Jian Wu, Philippe Traoré, Alberto T Pérez, and Pédro A Vázquez. On two-dimensional finite amplitude electro-convection in a dielectric liquid induced by a strong unipolar injection. *Journal of Electrostatics*, 74:85–95, 2015.
- [5] Yu Zhang, Lijuan Liu, Yang Chen, and Jiting Ouyang. Characteristics of ionic wind in needle-to-ring corona discharge. *Journal of Electrostatics*, 74:15–20, 2015.
- [6] Mengqi Zhang, Fulvio Martinelli, Jian Wu, Peter J Schmid, and Maurizio Quadrio. Modal and non-modal stability analysis of electrohydrodynamic flow with and without cross-flow. *Journal of Fluid Mechanics*, 770:319–349, 2015.
- [7] Xuerao He, Zhihao Sun, and Mengqi Zhang. Moffatt eddies in electrohydrodynamics flows: numerical simulations and analyses. *Journal of Fluid Mechanics*, 953:A14, 2022.
- [8] Wei Liu, Yueting Zhou, and Pengpeng Shi. Scaling laws of electroconvective flow with finite vortex height near permselective membranes. *Physical Review E*, 102(3):033102, 2020.
- [9] Wei Liu, Yueting Zhou, and Pengpeng Shi. Critical selection of shear sheltering in electroconvective flow from chaotic to steady state. *Journal of Fluid Mechanics*, 946:A3, 2022.
- [10] Xuerao He and Mengqi Zhang. On the flow instability under thermal and electric fields: A linear analysis. *European Journal of Mechanics-B/Fluids*, 88:34–46, 2021.
- [11] Ben Ma, Lei Wang, Kun He, and Dinggen Li. Electro-thermo-convection in power-law fluids within a square enclosure with an inner cylinder. *Physics of Fluids*, 33(8), 2021.

- [12] Guangze Liu, Yu Zhang, Dian Li, Yuxing Peng, and Jian Wu. Review on electro-convection and electro-thermo-convection in dielectric liquids within different geometrical models. *Journal of Electrostatics*, page 104089, 2025.
- [13] MJ Gross and JE Porter. Electrically induced convection in dielectric liquids. *Nature*, 212(5068):1343–1345, 1966.
- [14] F Pontiga, A Castellanos, and AT Richardson. The onset of overstable motions in a layer of dielectric liquid subjected to the simultaneous action of a weak unipolar injection of charge and a thermal gradient. *The Quarterly Journal of Mechanics and Applied Mathematics*, 45(1):25–46, 1992.
- [15] Kun He, Zhenhua Chai, Lei Wang, Ben Ma, and Baochang Shi. Numerical investigation of electro-thermo-convection with a solid-liquid interface via the lattice boltzmann method. *Physics of Fluids*, 33(3), 2021.
- [16] Z Wang, Y Tian, C Zhang, Y Wang, and W Deng. Massively multiplexed electrohydrodynamic tip streaming from a thin disc. *Physical Review Letters*, 126(6):064502, 2021.
- [17] Shiyuan Ma, Yifei Guan, and Jian Wu. Experimental study of heat transfer enhancement with point-to-ring corona discharge. *International Journal of Heat and Mass Transfer*, 184:122273, 2022.
- [18] Yifei Guan, Xuerao He, Qi Wang, Zhiwei Song, Mengqi Zhang, and Jian Wu. Monotonic instability and overstability in two-dimensional electrothermohydrodynamic flow. *Physical Review Fluids*, 6(1):013702, 2021.
- [19] Tian-Fu Li, Zheng-Gang Su, Kang Luo, and Hong-Liang Yi. Transition to chaos in electro-thermo-convection of a dielectric liquid in a square cavity. *Physics of Fluids*, 32(1), 2020.
- [20] Qi Wang, Yifei Guan, Tao Wei, and Jian Wu. Transition sequences and heat transfer enhancement in electro-thermo-convection of a dielectric liquid between two parallel electrodes. *International Journal of Thermal Sciences*, 179:107705, 2022.
- [21] A Kourmatzis and JS Shrimpton. Turbulent three-dimensional dielectric electrohydrodynamic convection between two plates. *Journal of Fluid Mechanics*, 696:228–262, 2012.

- [22] Yifei Guan, Qi Wang, Mengqi Zhang, Yu Zhang, and Jian Wu. Numerical investigation of two-dimensional electro-thermo-hydrodynamic turbulence: Energy budget and scaling law analysis. *International Journal of Heat and Mass Transfer*, 247:127094, 2025.
- [23] Antonio Castellanos and Pierre Atten. Numerical modeling of finite amplitude convection of liquids subjected to unipolar injection. *IEEE transactions on industry applications*, IA-23:825–830, 1987.
- [24] R Chicón, A Castellanos, and E Martin. Numerical modelling of coulomb-driven convection in insulating liquids. *Journal of Fluid Mechanics*, 344:43–66, 1997.
- [25] Ph. Traoré and A.T. Pérez. Two-dimensional numerical analysis of electroconvection in a dielectric liquid subjected to strong unipolar injection. *Physics of Fluids*, 24(3), 2012.
- [26] Jian Wu, Philippe Traoré, Pedro A Vázquez, and Alberto T Pérez. Onset of convection in a finite two-dimensional container due to unipolar injection of ions. *Physical Review E*, 88(5):053018, 2013.
- [27] Kang Luo, Jian Wu, Hong-Liang Yi, and He-Ping Tan. Lattice boltzmann model for coulomb-driven flows in dielectric liquids. *Physical Review E*, 93(2):023309, 2016.
- [28] Kang Luo, Jian Wu, Hong-Liang Yi, Lin-Hua Liu, and He-Ping Tan. Hexagonal convection patterns and their evolutionary scenarios in electroconvection induced by a strong unipolar injection. *Physical Review Fluids*, 3(5):053702, 2018.
- [29] Yifei Guan and Igor Novosselov. Two relaxation time lattice boltzmann method coupled to fast fourier transform poisson solver: Application to electroconvective flow. *Journal of computational physics*, 397:108830, 2019.
- [30] Yifei Guan and Igor Novosselov. Numerical analysis of electroconvection in cross-flow with unipolar charge injection. *Physical Review Fluids*, 4(10):103701, 2019.
- [31] Philip Holmes, John L Lumley, Gahl Berkooz, and Clarence W Rowley. *Turbulence, coherent structures, dynamical systems and symmetry*. Cambridge university press, 2012.

- [32] Kunihiko Taira, Steven L Brunton, Scott Dawson, Clarence W Rowley, Tim Colonius, Beverley J McKeon, Oliver T Schmidt, Stanislav Gordeyev, Vasilios Theofilis, and Lawrence S Ukeiley. Modal analysis of fluid flows: An overview. *AIAA Journal*, 55(12):4013–4041, 2017.
- [33] Kunihiko Taira, Maziar S Hemati, Steven L Brunton, Yiyang Sun, Karthik Duraisamy, Shervin Bagheri, Scott Dawson, and Chi-An Yeh. Modal analysis of fluid flows: Applications and outlook. *AIAA Journal*, 58(3):998–1022, 2020.
- [34] Steven L Brunton and J Nathan Kutz. *Data-driven science and engineering: Machine learning, dynamical systems, and control*. Cambridge University Press, 2019.
- [35] Steven L. Brunton, Bernd R. Noack, and Petros Koumoutsakos. Machine learning for fluid mechanics. *Annual Review of Fluid Mechanics*, 52:477–508, 2020.
- [36] Edward N Lorenz. Deterministic nonperiodic flow. *Journal of the atmospheric sciences*, 20(2):130–141, 1963.
- [37] Barry Saltzman. Finite amplitude free convection as an initial value problem. *Journal of the Atmospheric Sciences*, 19(4):329–341, 1962.
- [38] JL Lumley. The structure of inhomogeneous turbulence. atmospheric turbulence and wave propagation. *AM Yaglom, VI Tatarski*, pages 166–178, 1967.
- [39] Gal Berkooz, Philip Holmes, and John L Lumley. The proper orthogonal decomposition in the analysis of turbulent flows. *Annual review of fluid mechanics*, 25(1):539–575, 1993.
- [40] John L Lumley. *Stochastic tools in turbulence*. Courier Corporation, 2007.
- [41] J Nathan Kutz, Steven L Brunton, Bingni W Brunton, and Joshua L Proctor. *Dynamic mode decomposition: data-driven modeling of complex systems*. SIAM, 2016.
- [42] Kazufumi Ito and Sivaguru S Ravindran. A reduced-order method for simulation and control of fluid flows. *Journal of computational physics*, 143(2):403–425, 1998.

- [43] Bernd R Noack, Marek Morzynski, and Gilead Tadmor. *Reduced-order modelling for flow control*, volume 528. Springer Science & Business Media, 2011.
- [44] Arvind T Mohan and Datta V Gaitonde. A deep learning based approach to reduced order modeling for turbulent flow control using lstm neural networks. *arXiv preprint arXiv:1804.09269*, 2018.
- [45] Qun Chao, Zi Xu, Yuechen Shao, Jianfeng Tao, Chengliang Liu, and Shuo Ding. Hybrid model-driven and data-driven approach for the health assessment of axial piston pumps. *International Journal of Hydromechanics*, 6(1):76–92, 2023.
- [46] Changsheng Xi, Jie Yang, Xiaoxia Liang, Rahizar Bin Ramli, Shaoning Tian, Guojin Feng, and Dong Zhen. An improved gated convolutional neural network for rolling bearing fault diagnosis with imbalanced data. *International Journal of Hydromechanics*, 6(2):108–132, 2023.
- [47] Omer A Alawi, Haslinda Mohamed Kamar, Mustafa Mudhafar Shawkat, Mohammed M Al-Ani, Hussein A Mohammed, Raad Z Homod, and Mazlan A Wahid. Artificial intelligence-based viscosity prediction of polyalphaolefin-boron nitride nanofluids. *International Journal of Hydromechanics*, 7(2):89–112, 2024.
- [48] Eduardo Henrique Taube Cunegatto, Flávia Schwarz Franceschini Zinani, and Sandro José Rigo. Multi-objective optimisation of micromixer design using genetic algorithms and multi-criteria decision-making algorithms. *International Journal of Hydromechanics*, 7(3):224–249, 2024.
- [49] Kunihiko Taira, Steven L Brunton, Scott TM Dawson, Clarence W Rowley, Tim Colonius, Beverley J McKeon, Oliver T Schmidt, Stanislav Gordeyev, Vassilios Theofilis, and Lawrence S Ukeiley. Modal analysis of fluid flows: An overview. *AIAA journal*, 55(12):4013–4041, 2017.
- [50] Dulakshi SK Karunasinghe and Shie-Yui Liong. Chaotic time series prediction with a global model: Artificial neural network. *Journal of Hydrology*, 323(1-4):92–105, 2006.
- [51] Ashesh Chattopadhyay, Pedram Hassanzadeh, and Devika Subramanian. Data-driven prediction of a multi-scale lorenz 96 chaotic system using deep

- learning methods: Reservoir computing, ann, and rnn-lstm. *Nonlinear Processes in Geophysics Discussions*, 2020:1–26, 2020.
- [52] Zhixin Lu, Jaideep Pathak, Brian Hunt, Michelle Girvan, Roger Brockett, and Edward Ott. Reservoir observers: Model-free inference of unmeasured variables in chaotic systems. *Chaos: An Interdisciplinary Journal of Nonlinear Science*, 27(4), 2017.
- [53] Thomas L Carroll. Using reservoir computers to distinguish chaotic signals. *Physical Review E*, 98(5):052209, 2018.
- [54] Chad Nathe, Chandra Pappu, Nicholas A Mecholsky, Joe Hart, Thomas Carroll, and Francesco Sorrentino. Reservoir computing with noise. *Chaos: An Interdisciplinary Journal of Nonlinear Science*, 33(4), 2023.
- [55] Jia-Shu Zhang and Xian-Ci Xiao. Predicting chaotic time series using recurrent neural network. *Chinese Physics Letters*, 17(2):88, 2000.
- [56] Qinghai Li and Rui-Chang Lin. A new approach for chaotic time series prediction using recurrent neural network. *Mathematical Problems in Engineering*, 2016(1):3542898, 2016.
- [57] Alex Graves. Long short-term memory. *Supervised sequence labelling with recurrent neural networks*, pages 37–45, 2012.
- [58] Pantelis R Vlachas, Wonmin Byeon, Zhong Y Wan, Themistoklis P Sapsis, and Petros Koumoutsakos. Data-driven forecasting of high-dimensional chaotic systems with long short-term memory networks. *Proceedings of the Royal Society A: Mathematical, Physical and Engineering Sciences*, 474(2213):20170844, 2018.
- [59] Milad Keshtkar Langeroudi, Mohammad Reza Yamaghani, and Siavash Khodaparast. Fd-lstm: A fuzzy lstm model for chaotic time-series prediction. *IEEE intelligent systems*, 37(4):70–78, 2022.
- [60] Yifei Guan, Ashesh Chattopadhyay, Adam Subel, and Pedram Hassanzadeh. Stable a posteriori LES of 2D turbulence using convolutional neural networks: Backscattering analysis and generalization to higher Re via transfer learning. *Journal of Computational Physics*, 458:111090, 2022.

- [61] Kraig B Winters, Peter N Lombard, James J Riley, and Eric A D’Asaro. Available potential energy and mixing in density-stratified fluids. *Journal of Fluid Mechanics*, 289:115–128, 1995.
- [62] Graham O Hughes, Bishakhdat Gayen, and Ross W Griffiths. Available potential energy in rayleigh–bénard convection. *Journal of Fluid Mechanics*, 729:R3, 2013.
- [63] Yu Zhang, Di-Lin Chen, Xiao-Ping Luo, Kang Luo, Jian Wu, and Hong-Liang Yi. Coulomb-driven electroconvection turbulence in two-dimensional cavity. *Journal of Fluid Mechanics*, 980:A22, 2024.
- [64] Lloyd N. Trefethen. *Spectral methods in MATLAB*. Society for Industrial and Applied Mathematics, USA, 2000.
- [65] Randall J LeVeque. *Finite difference methods for ordinary and partial differential equations: steady-state and time-dependent problems*. SIAM, 2007.
- [66] Tobin A Driscoll, Nicholas Hale, and Lloyd N Trefethen. *Chebfun guide*, 2014.
- [67] Stephane Mallat. *A wavelet tour of signal processing*. Academic Press, 1999.
- [68] Desmond J Higham and Nicholas J Higham. *MATLAB guide*. SIAM, 2016.
- [69] Yifei Guan, Steven L Brunton, and Igor Novosselov. Sparse nonlinear models of chaotic electroconvection. *Royal Society Open Science*, 8(8):202367, 2021.
- [70] Siegfried Grossmann and Detlef Lohse. Scaling in thermal convection: a unifying theory. *Journal of Fluid Mechanics*, 407:27–56, 2000.
- [71] Peter Alan Davidson. *Turbulence: an introduction for scientists and engineers*. Oxford university press, 2015.